Full Paper

Wiley Online Library

ELECTROANALYSIS

DOI: 10.1002/elan.202060406

Adsorption, Thermodynamic, and Experimental Studies of Corrosion Inhibitor of Tin in 0.2 M Maleic Acid by Hydrogen Phosphate Ions (HPO_4^{2-})

Brahim Ait Addi,[a] Abdelaziz Ait Addi,[a] Abdul Shaban,*[b] El-Habib Ait Addi,[c] and Mohamed Hamdani[a]

Abstract: The inhibition efficiency of $H_2PO_4^{2-}$ ions against tin corrosion in 0.2 M maleic acid is studied using electrochemical methods, surface analytical methods, and thermodynamic analysis. The potentiodynamic polarization plots showed the presence of an active/passive transition state of the tin electrode. The EIS measurements confirmed that the inhibition efficiency of $H_2PO_4^{2-}$ increased by increasing the concentration ($\eta = 81\,\%$ at $C_{inh} = 2.10^{-2}$ M) and decreased by rising the temperature. The polarization tests demonstrated that the inhibitor performs as a cathodic-type. The adsorption of the inhibitor was spontaneous and followed the Langmuir adsorption isotherm. A model of the inhibition mechanism was suggested.

Keywords: Corrosion inhibition · Polarization Curves · EIS · Tin · Hydrogen phosphate ions · Maleic Acid

1 Introduction

Corrosion in the food industry is an important matter since it can cause expensive production-interruptions, and more serious consequence the safety and quality assurances of the foodstuffs. The corrosive environment in the food and beverage manufacturing includes moderately to exceedingly concentrated chloride environment often assorted with substantial organic acid quantities [1].

Some types of foodstuff packaging such as metal cans involve the usage of coatings to safeguard against metal corrosion. The low strength of tin (Sn) limited its applications in many industries. Nevertheless, in the food industry where manufacturing of steel cans, Sn protective coatings are wildly applied [1]. Over a century, tinplate, a steel sheet coated with pure tin, has been extensively applied in the manufacturing of foodstuff and beverage containers [2].

Attributed to the extensive applications of Sn in soft solders, dental amalgam, and tinplate, the electrochemical characterization of Sn in aqueous solutions is of great importance [1,2]. Therefore, considerable attention must be paid to the electrochemical corrosion and passivation processes of Sn in an environment containing different acids (such as carboxylic and fruit acids).

For the purpose to protect the flavor and appearance of packaged foodstuff from oxidative degradation, the inner surface of food containers must be coated by a thin Sn coating. As a result of the corrosion process, foodstuff can get contaminated by Sn, despite the fact it is not listed as a toxic metal, a considerably large dosage can cause serious digestive disturbances [2].

Nevertheless, the exposition to aggressive surroundings in the course of long-term service, the metal tends to lose its corrosion resistance capability, which leads to the deterioration of its surface and affecting the metal durability causing severe financial damages and contamination of the environment [3,4]. Tin dissolution in the presence of carboxylic acid, especially from the inside of a can body into the food content, has a major influence on the food quality and may cause toxicological effects [5].

The costly corrosion damages can be hindered by using numerous procedures such as materials selection, process control, and the application of inhibitors [6,7]. Between these approaches, the application of corrosion inhibitors is the most practical alternative to stop the damage to the metal surface in corrosive media. The function of inhibitors is to hinder the metal corrosion processes by either altering the anodic or cathodic polarization activities (Tafel slopes), isolating the metal surface

[a] B. Ait Addi, A. Ait Addi, M. Hamdani
Team of Physical Chemistry and Environment, Faculty of Science, Ibn Zohr University,
Agadir, Morocco
[b] A. Shaban
Institute of Materials and Environmental Chemistry, Research Centre for Natural Sciences, Hungarian Academy of Sciences, Bp., Hungary
E-mail: shaban.abdul@ttk.mta.hu
[c] E.-H. Ait Addi
Research Group: Process and Chemical Engineering, Agadir School of Technology,
Ibn Zohr University, Agadir, Morocco

© 2020 The Authors. Published by Wiley-VCH GmbH. This is an open access article under the terms of the Creative Commons Attribution Non-Commercial NoDerivs License, which permits use and distribution in any medium, provided the original work is properly cited, the use is non-commercial and no modifications or adaptations are made.

from the corrosive ions (diffusion control), or increasing the electrical resistance of the metal surface.

In recent years, due to stricter environmental restriction inhibitors must fulfill the criteria of being safe and environmentally friendly [8], which banned toxic inhibitor compositions such as sodium nitrite ($NaNO_2$) [9,10]. Phosphates, being inexpensive and effective, have been studied substantially as metallic corrosion inhibitor [11–14]. Even though phosphate compounds are extensively studied as potential corrosion inhibitors but their inhibition mechanism is still not elucidated [15,16]. Some researchers have recommended that the phosphate ions combine with Fe^{3+} and Fe^{2+} to formulate the insoluble ferric and soluble ferrous phosphates, respectively [8,11]. The formation of ferrous phosphate leads to a decrease in the phosphate ions concentration and an increase in the pH value at the metal/solution interface.

Electrochemical techniques (*dc* and *ac*), potentiodynamic (polarization curves), and electrochemical impedance spectroscopy (EIS), have been extensively applied in the field of inhibitor evaluations [8,17]. Surface analytical analysis (scanning electron microscopy (SEM) and energy-dispersive X-ray spectroscopy (EDX) can obtain valuable information on the morphology and composition of the surface coating of the metal [18].

The present contribution aims to examine the electrochemical behavior of the Sn electrode in 0.2 M maleic acid solution under different circumstances such as hydrogen phosphate ions concentration and solution temperature. Electrochemical techniques (potentiodynamic polarization and electrochemical impedance spectroscopy (EIS)) are used. The temperature influence on the effectiveness of the tested inhibitor against Sn corrosion in a 0.2 M maleic acid solution was studied in the range of 293–333 K.

2 Experimental

2.1 Materials and Electrodes

The investigations were performed in a 0.2 M maleic acid solution without or with various concentrations of Na_2HPO_4 as potential corrosion inhibitors. All applied solutions were prepared from analytical grade chemicals (p.a. Merck) and doubly distilled water and were deaerated by bubbling nitrogen through the cell. The working electrode (WE) was prepared from a tin rod (Aldrich 99.99 %), axially embedded in Araldite epoxy resin holders restricting the uncovered circular area (0.8 cm^2). The WE surface was polished with different grades of SiC emery papers (down to 1200 in grit size), degreased with acetone, and immediately rinsed with bidistilled water. For the electrochemical measurements, the used inhibitor concentrations were: 10^{-3}, 10^{-2}, and 2.10^{-2} M.

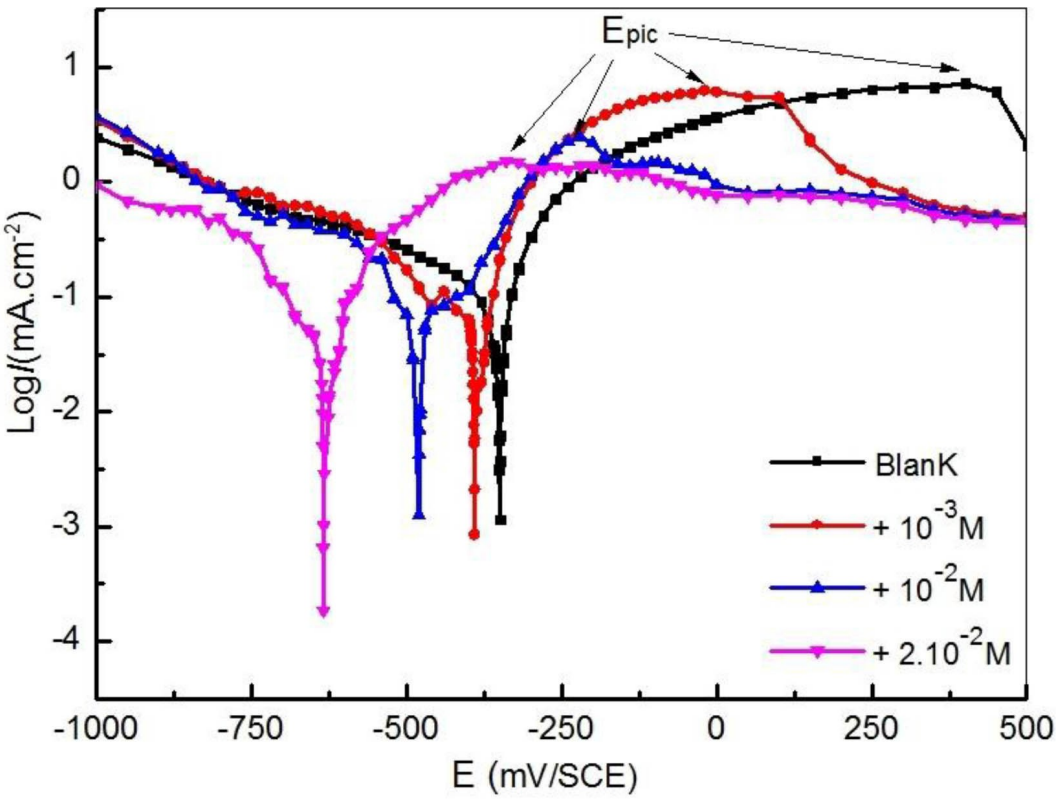

Fig. 1. Polarization curves for Sn electrode in 0.2 M maleic acid containing different C_{inh} of HPO_4^{2-} at 293 K.

© 2020 The Authors. Published by Wiley-VCH GmbH

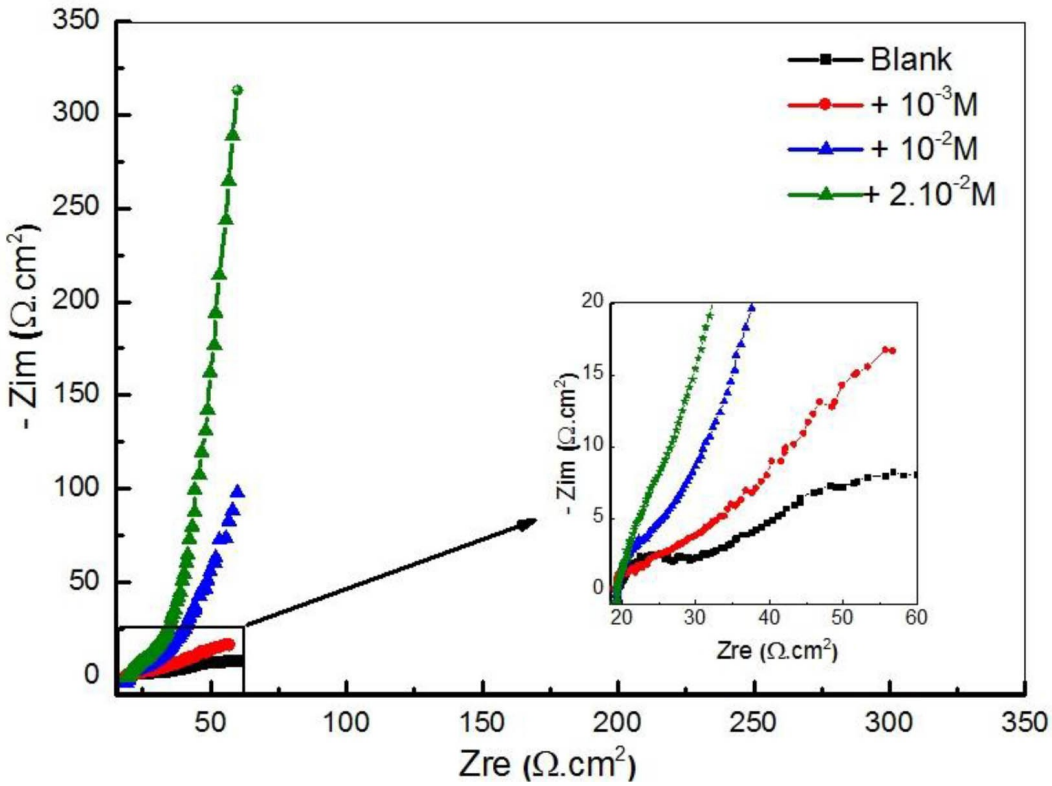

Fig. 2. Nyquist plot for Sn in 0.2 M maleic acid with and without different C_{inh} of HPO_4^{2-} at 293 K

2.2 Electrochemical Measurements

Electrochemical measurements were carried out in a conventional cylindrical three-electrode tempered glass cell that is thermostated with double-wall (Tacussel Standard CEC/TH). The reference and Auxiliary electrodes were a saturated calomel electrode (SCE) and Pt sheet, respectively. The experiments were performed by using Radiometer-Analytical (potentiostat/galvanostat-PGZ 100), controlled by Volta-Master v.4 software.

Potentiodynamic polarization curves were recorded at a potential scan rate of 60 mV/min. An immersion time of 1 hr. was allowed, to reach the open circuit potential (OCP), before both the potentiodynamic polarization and EIS experiments. Tafel runs were conducted in the potential range from −900 mV to 0 mV relative to the OCP, at a scan rate of 1 $mV.s^{-1}$. The Tafel extrapolation method was implemented in the calculation of corrosion current densities and other Tafel fit parameters.

The EIS experiments were made using a sinusoidal wave voltage signal (10 mV amplitude) applied to the WE while the current is measured at different frequencies, (from 100 kHz to 100 mHz), at OCP. All electrochemical experiments were performed at a temperature of 293 K and pH = 1.8 (±0.2) in 0.2 M maleic acid at various concentrations of hydrogen phosphate ions (10^{-3}, 10^{-2}, and 2.10^{-2} M).

2.3 Surface Characterization

The surface analysis of the Sn specimen was conducted by placing the cleaned samples in 0.2 M maleic acid with and without the inhibitors for 24 h immersion time, then washing and drying them. Scanning electron microscopy (SEM) and energy dispersive X-ray (EDX) analysis were performed.

3 Results and Discussion

3.1 Effect of HPO_4^{2-} on the Electrochemical Behavior of Sn

3.1.1 Potentiodynamic Polarization Measurements

Figure 1 shows the cathodic and anodic polarization plots of Sn immersed in 0.2 M maleic acid solution at 293 K in the absence and presence of different concentrations of HPO_4^{2-}. Electrochemical parameters such as corrosion potential (E_{corr}), cathodic Tafel slopes (b_c), and corrosion current density (I_{corr}) obtained by extrapolation of the cathodic regions of the Tafel plots and inhibition efficiency were listed in Table 1.

It is noticeable that the addition of HPO_4^{2-} suppressed the cathodic reaction, as seen in Figure 1, i.e. the inhibitor hindered the hydrogen reduction reaction at the cathodic sites. Alternatively, assessment of the anodic branch revealed that tin exhibited a field of activity (activity peaks) in the presence of the HPO_4^{2-} ions, followed by a

© 2020 The Authors. Published by Wiley-VCH GmbH

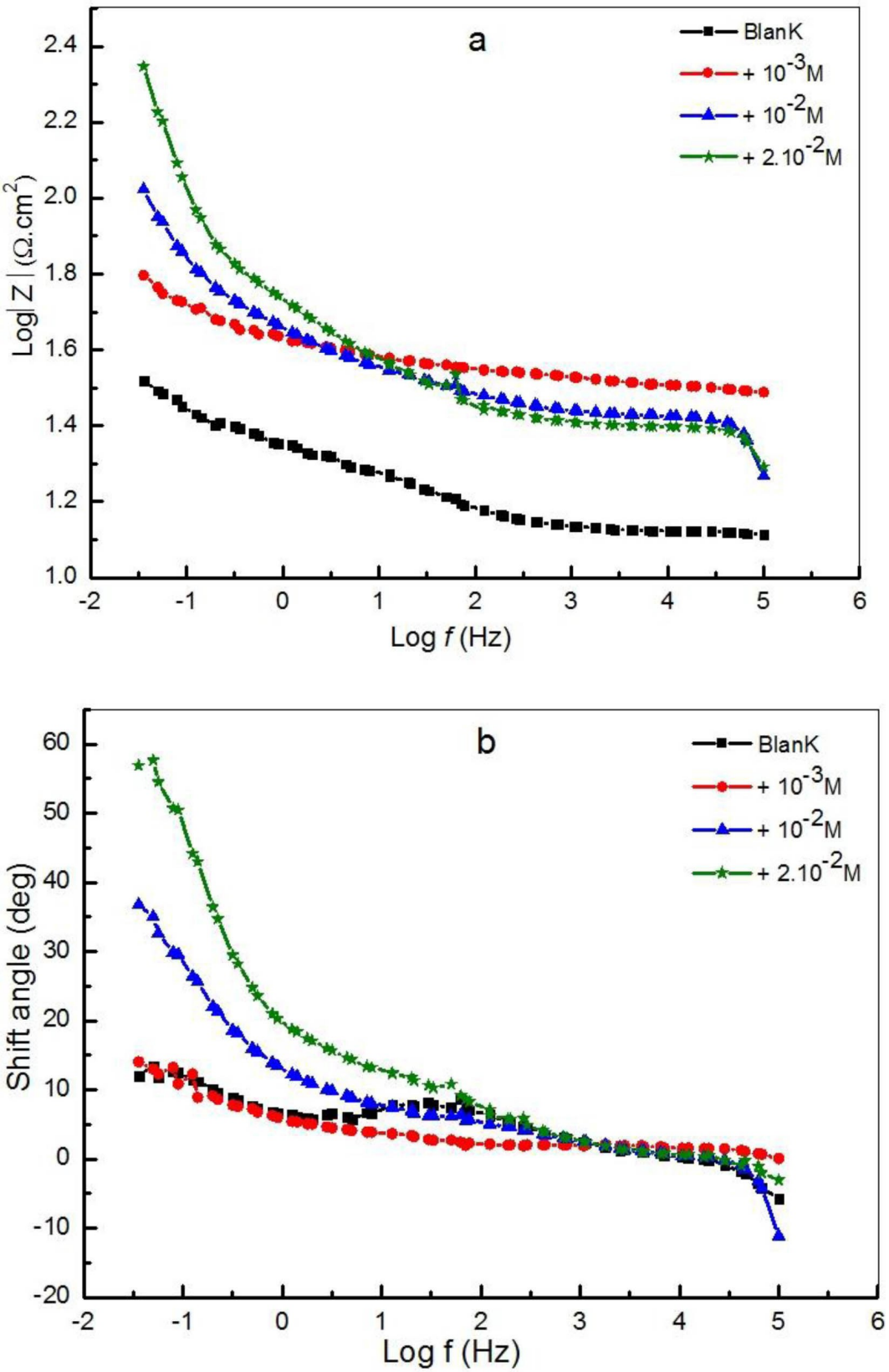

Fig. 3. Bode-modulus plots for Sn in 0.2 M maleic acid with and without different C_{inh} of HPO_4^{2-} at 293 K: (**a**) Log Z vs. Log f and (**b**) phase shift (φ) vs. Log f.

© 2020 The Authors. Published by Wiley-VCH GmbH

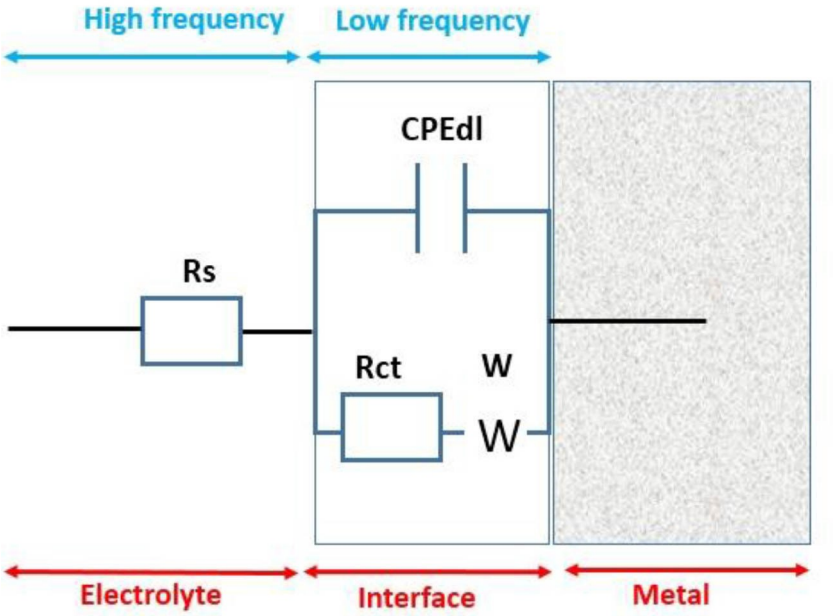

Fig. 4. Electrical circuit equivalent of Sn in 0.2 M maleic acid solution in the presence of C_{inh} of HPO_4^{2-}.

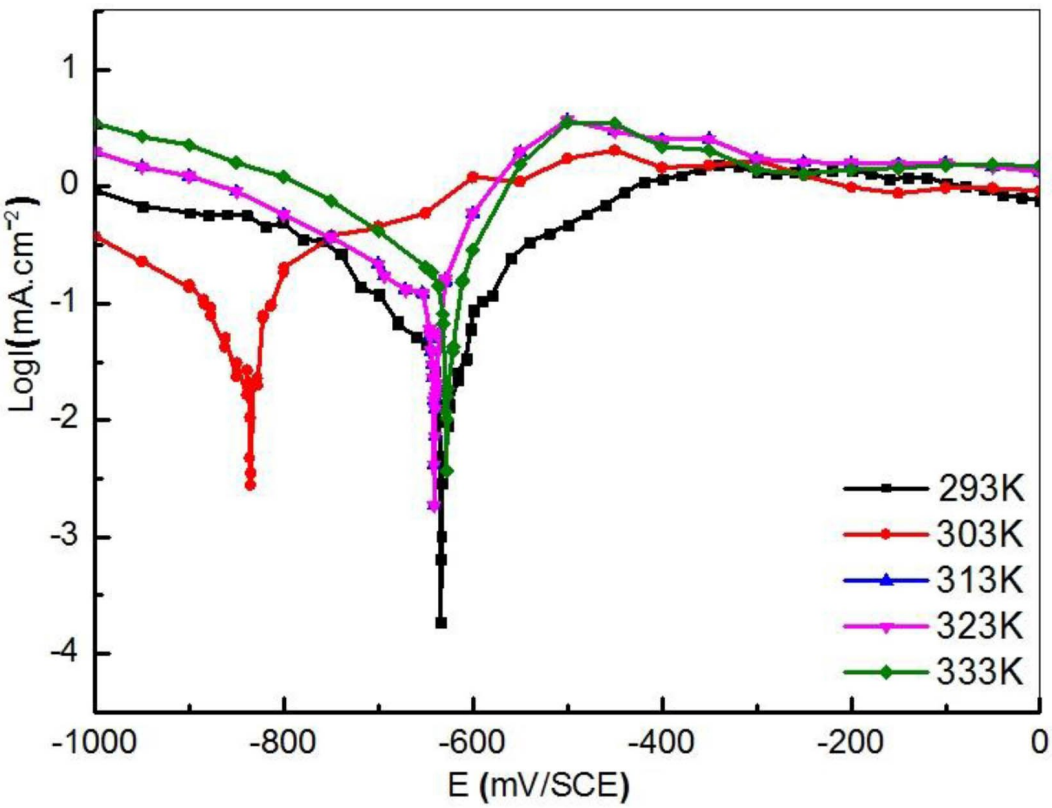

Fig. 5. Polarization curves for Sn in 0.2 M maleic acid containing 0.02 M of HPO_4^{2-} at different temperatures.

some-how passivation range breaking due to localized attack. Nevertheless, as shown in Table 1, the results showed that the addition of HPO_4^{2-} ions displace the values of peaks potentials activation E_{pic} in the direction of more active values accompanied by a slight decrease in the intensities of the peaks upon increasing C_{inh} of HPO_4^{2-}.

© 2020 The Authors. Published by Wiley-VCH GmbH

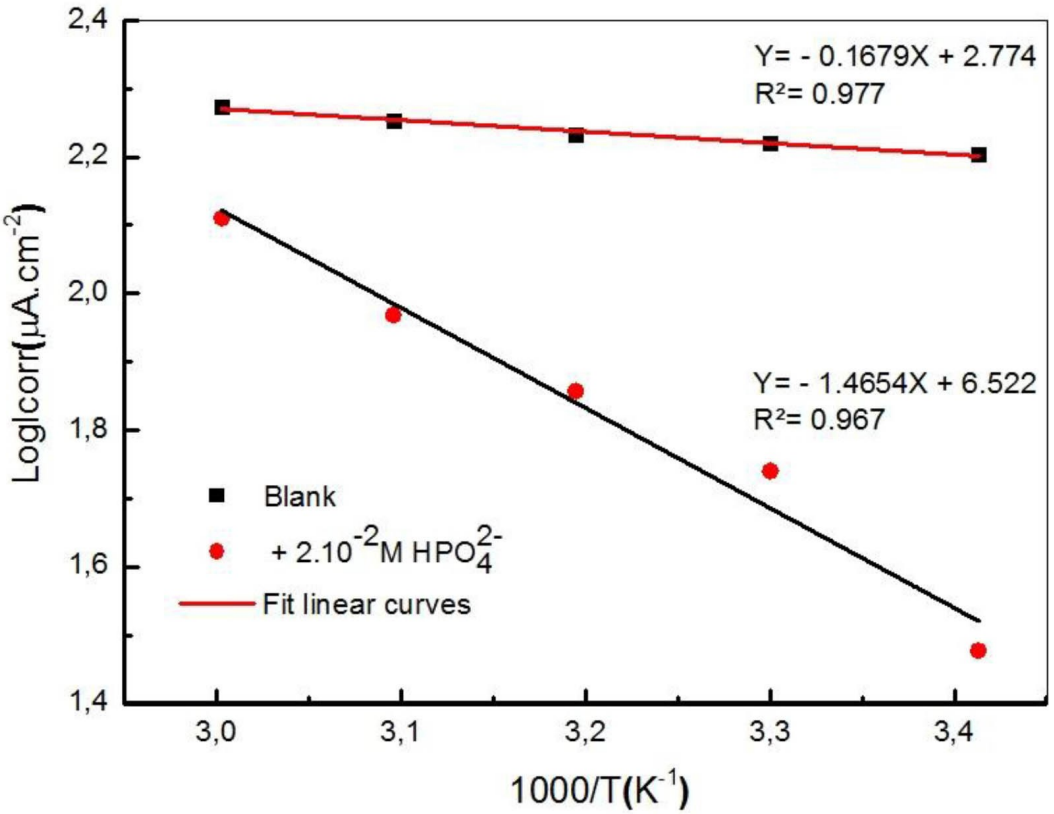

Fig. 6. Arrhenius plots of Log (i_{corr}) versus 1000/T for Sn in 0.2 M maleic acid without and with the addition of 0.02 M HPO_4^{2-}

The most significant shift of E_{corr} is achieved in the case of $C_{inh} = 10^{-2}$ M of HPO_4^{2-}. This action indicates that the HPO_4^{2-} ions obstruct tin dissolution. In the literature, it was estimated that E_{corr} shift value of 85 mV between the uninhibited and inhibited solution is the basis for categorizing an inhibitor as either anodic, cathodic, or mixed-type inhibitor [19]. As shown in Table 1, the E_{corr} shift values obtained vary from −348 mV to −637 mV (to more cathodic), which proves that HPO_4^{2-} demonstrated a cathodic-type of inhibition.

The inhibition efficiency of an inhibitor, in protecting the metal surface from acid-induced corrosion, depends on the ability of its inhibitive species to adsorb on the metal surface to isolate the metal surface from the corrosive medium [20].

The corrosion inhibition efficiency (η %) is calculated using the following formula:

$$\eta\% = \frac{(I_{corr} - I_{corr-inh})}{I_{corr}} x100 \quad (1)$$

where $I_{corr-inh}$ and I_{corr} are the corrosion current density values with and without the addition of the inhibitor, respectively, extrapolated from cathodic Tafel lines to E_{corr}. The attained results visibly illustrate that η increases with increasing the C_{inh} of the inhibitor ions. This could be explained based on the adsorption of HPO_4^{2-} on the Sn surface and the adsorption process increased at higher inhibitor concentrations, respectively avoiding the aggressive attack on the Sn electrode by the maleic acid ions. The maximum inhibition efficiency for the tested inhibitor was (η = 81 %), established at C_{inh} = 0.02 M.

Table 1. Electrochemical parameters and the inhibition efficiency of Sn electrode corrosion in 0.2 M maleic acid containing different C_{inh} of HPO_4^{2-} at 293 K.

C_{inh} (M)	E_{corr} (mV)	E_{pic} (mV)	I_{pic} (A_1) (mA/cm²)	I_{corr} (µA/cm²)	−βc (mV/dec)	η (%)
0	−348	210.4	7.43	160	404	–
1.10^{-3}	−358	−162.3	6.08	110	359	31.2
1.10^{-2}	−480	−426.3	2.33	65	485	59.3
2.10^{-2}	−637	−343.1	1.48	30	339.5	81.2

© 2020 The Authors. Published by Wiley-VCH GmbH

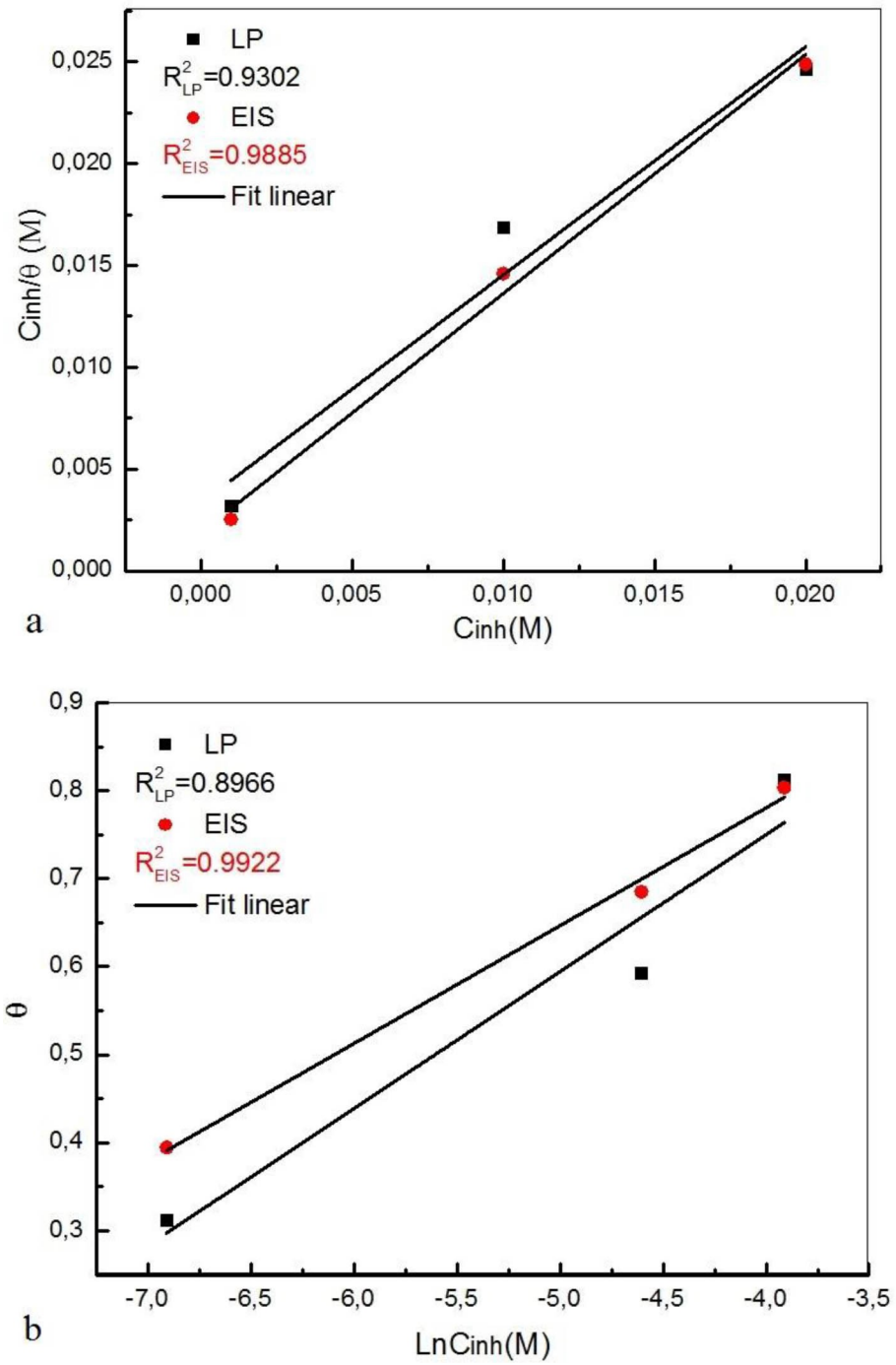

Fig. 7. Adsorption isotherms for Sn electrode in 0.2 M n in 0.2 M maleic acid containing different C_{inh} of HPO_4^{2-} at 293 K. (**a**) Langmuir adsorption, (**b**) Temkin adsorption.

3.1.2 EIS Results

EIS is employed to gain more profound information into the electrochemical processes of corrosion inhibition. EIS results, performed at OCP, are typically symbolized by Nyquist (aka Cole-Cole representation) and Bode plots. In the Nyquist plot usually, the negative value of the imaginary part of the impedance (y-axis) is plotted against the real part of the impedance (x-axis). The plot starts with high-frequency values. The other EIS widespread presentation technique is the Bode plot, where both the absolute values of the impedance and the phase-shift are plotted on the (y-axis) versus the log frequency on the (x-axis). The Bode plot demonstrates frequency dependence information where the Nyquist presentation does not involve frequency.

To interpret the EIS data, a correlation between the measured impedance data and an equivalent circuit

© 2020 The Authors. Published by Wiley-VCH GmbH

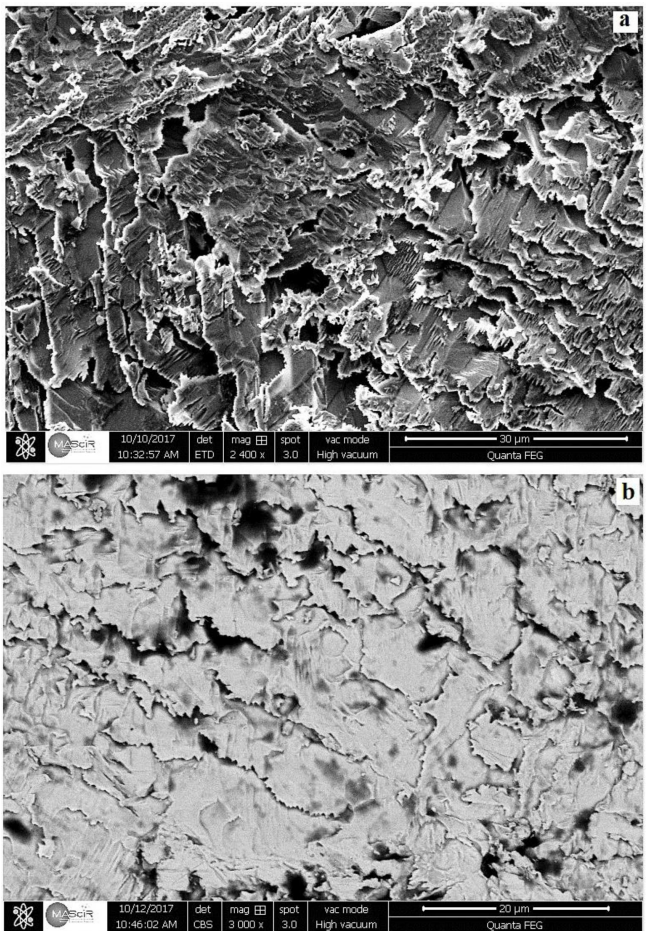

Fig. 8. SEM images of the Sn electrode in 0.2 M maleic acid solution (**a**) in the absence and (**b**) in the presence of 0.02 M HPO_4^{2-}.

demonstrating the physical corrosion or inhibition mechanism of the tested process, is implementd. Fitting the Nyquist plots to a proposed equivalent circuit model permits the physical understanding of the processes involved.

Figures 2 and 3 display the Nyquist and Bode-modulus spectra of the EIS tests on the tin electrode in a 0.2 M maleic acid solution with and without the addition of different C_{inh} of HPO_4^{2-}, respectively. Electrochemical data derived from EIS spectra, Figure 2, are presented in Table 2. These values are obtained by simulating the acquired experimental data against the proper electrical circuit using Z-view software. The η (%) was calculated from charge transfer resistance (polarization resistance, R_{ct}) values using the following Eq.:

$$\eta(\%) = \frac{R_{ct(inh)} - R_{ct}}{R_{ct}} \times 100 \quad (2)$$

where $R_{ct(inh)}$ and R_{ct} are the charge transfer resistance with and without the inhibitor, respectively. Eq. (2) expresses that when the diameter of the semicircle is high thus the polarization resistance (R_{ct}) will be high which consequently means lower corrosion rate.

The Nyquist impedance presentation (Figure 2), demonstrates two distinctive sections existing at the high and low-frequencies regions.

At the high-frequency region, a semicircle was obtained which elucidates the capacitive loop, which is characterized by the charge transfer resistance (R_{tc}) and the double layer capacitor (C_{dl}). At the low frequencies, the linear region is associated with the Warburg diffusional process through the liquid inter-phase [21]. The values of the double-layer capacitance were obtained at the maximum frequency (f_{max}), at which the imaginary component of the Nyquist plot is maximal, and calculated using Eq. 3:

$$C_{dl} = \frac{1}{2\pi f_{max} R_t} \quad (3)$$

Figure 2 displays the Nyquist presentation with a depressed capacitive loop at low frequencies, which is normally linked with the inhomogeneous Sn metal surface, characterized by the constant phase element (CPE). We observed that the inhibitor addition did not alter the profile of the EIS spectra relative with the spectra of the blank solution. This notice might indicate that the mechanisms of Sn corrosion and its inhibition processes did not alter significantly.

The analysis of the Bode-modulus plot (Figure 3) shows that the charge transfer resistance R_{ct} obtained from the impedance module at low-frequency increases gradually with the concentration of HPO_4^{2-}.

Experimental EIS data were fitted, to the equivalent electrical circuit schemed in Figure 4, using the EIS data fitting software (EC-Lab Software, V. 10.38). Figure 4 displays the equivalent circuit elements: R_s represents the solution resistance; R_{ct} is the charge transfer resistance also known as the polarization resistance; CPE_{dl} is the constant phase element; W denotes the Warburg's diffusion impedance element. The fitting procedure produced calculated results that are in acceptable agreement with the experimental impedance data, with $\chi^2 < 0.001$.

Analyzing the parameters associated with the EIS measurements of Sn in 0.2 M maleic acid solution with the addition of HPO_4^{2-} shows that as the inhibitor concentration increases: the charge transfer resistance R_{ct} increases (18.43 to 64.94 Ω), whereas C_{dl} decreases (918.51

Table 2. EIS parameters for Sn electrode in 0.2 M maleic acid with and without different C_{inh} of HPO_4^{2-} at 293 K obtained from Figure 2.

C_{inh} (M)	R_s (Ωcm^2)	R_{ct} (Ωcm^2)	C_{dl} ($\mu F cm^{-2}$)	η (%)
0	9.89	18.43	918.51	–
1.10^{-3}	30.80	30.44	530.63	39.45
1.10^{-2}	15.43	58.51	63.672	68.50
2.10^{-2}	13.24	64.94	30.609	80.33

© 2020 The Authors. Published by Wiley-VCH GmbH

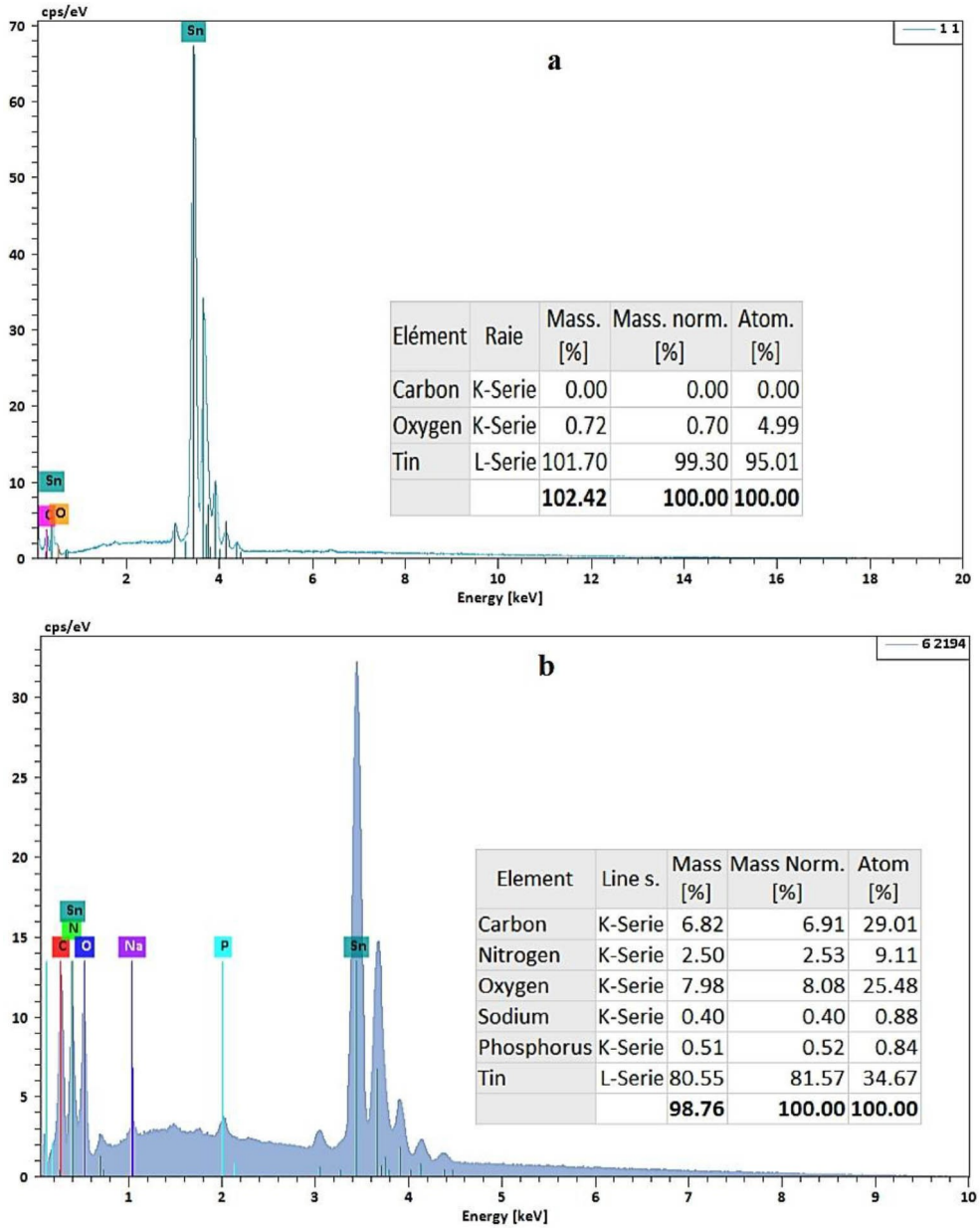

Fig. 9. EDX analysis of the surface of the Sn electrode in 0.2 M maleic acid (**a**) in the absence and (**b**) in the presence of 0.02 M HPO_4^{2-}.

to 30.61 μF) as shown in Table 2. That results can be attributed to the formation of a protective complex film due to the HPO_4^{2-} ions absorption on the Sn surface or loss of the dielectric constant, which increases the effectiveness of the inhibitor [22].

In Table 2, we can observe that the values of C_{dl} decrease in the presence of HPO_4^{2-} relative to the blank solution, suggesting inhibitor ions adsorption on the tin surface. Additionally, in inhibited media, an increase of charge-transfer-resistance (R_{ct}) is obtained, demonstrating the performance of the inhibitor ions to hinder the dissolution rate of Sn in 0.2 M maleic acid.

The highest reported (η) value (≈81 %) was obtained in the case of 0.02 M HPO_4^{2-}. The achieved inhibition efficiency values based on *ac* (EIS) and the *dc* potentiodynamic polarization (PDP) methods are slightly different at the middle concentration but are similar at higher concentrations; which showed a decent agreement among the applied electrochemical methods.

© 2020 The Authors. Published by Wiley-VCH GmbH

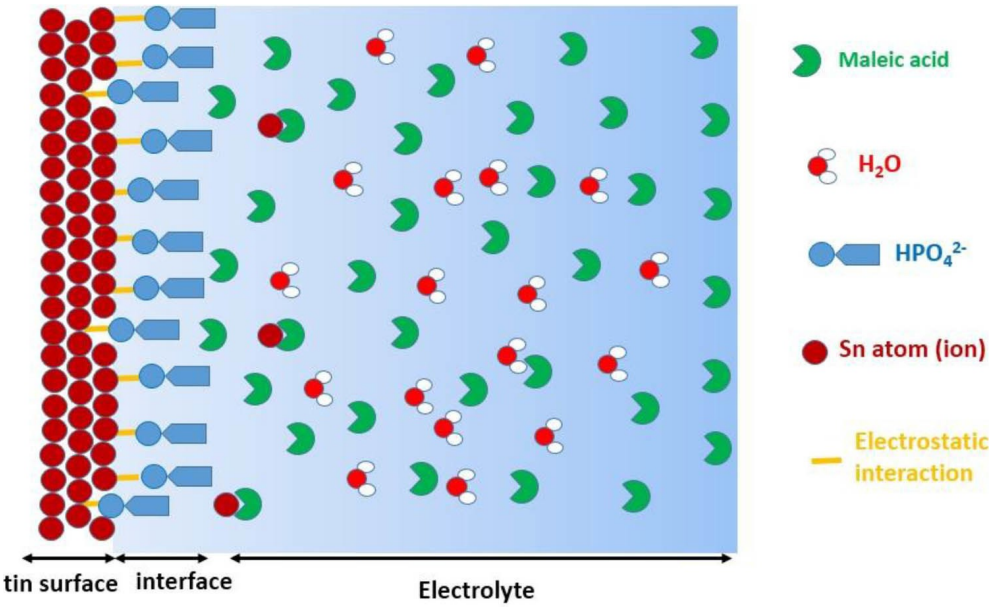

Fig. 10. Schematic diagram of the proposed mechanism action of HPO_4^{2-} on tin surface.

3.2 Thermodynamic Analysis

3.2.1 Effect of Temperature on the Inhibition Effect of HPO_4^{2-}

Temperature is a key factor in the inhibition processes. It can modify the metal-inhibitor interaction in the corrosive medium and inform the mode of adsorption of the inhibitor. Figure 5 shows the potentiodynamic polarization results of the effect of temperature on Sn corrosion in 0.2 M maleic acid solution in the presence of 0.02 M HPO_4^{2-} studied in the temperature range 293–333 K. The corrosion kinetic parameters, such as corrosion current density I_{corr}, corrosion potential E_{corr}, and the cathodic Tafel slope (b_c), were collected from the curves of Figure 5 and tabulated in Table 3.

As can be observed in Figure 5, the curves demonstrated the visibility of the Tafel regions with an increase in the anodic and cathodic current densities as a result of increasing the solution temperature. The cathodic curves (reduction region) are parallel, indicating that the reduction of H^+ ions on the tin surface is performed according to a similar activation mechanism at all temperatures.

Table 3. Polarization parameters of Sn in 0.2 M maleic acid at different temperatures obtained from Figure 5.

	T (K)	E_{corr} (mV)	I_{corr} (μA/cm^2)	$-\beta_a$ (mV/dec)	η (%)
2.10^{-2} M HPO_4^{2-}	293	−637	30	339.5	81
	303	−798	55	224	66
	313	−634	72	224	57
	323	−776	93	284	48
	333	−768	129	391	31

The data in Table 3 show clearly that the current densities increase with raising the temperature. The values of the HPO_4^{2-} inhibition efficiency against Sn corrosion in 0.2 M maleic acid at different solution temperatures declined sharply as the temperature of the solution was increased. Correspondingly, a decrease in η for 0.02 M HPO_4^{2-} inhibitor in 0.2 M maleic acid medium decreased from 81 to 31 % for temperatures of 293 and 333 K, respectively.

3.2.2 Activation Thermodynamic Parameters

Corrosion is the consequence of the interaction between a metal surface and its surroundings which might alter the metal properties. This metal/interface interaction is normally in an electrochemical process form thus thermodynamic and kinetic treatments and considerations can be applied [23].

To further gain information on the metal corrosion inhibition mechanism, the approach of the activation energy (E_a) determination by the use of the Arrhenius relationship between the metal corrosion current and the solution temperature, without and with the presence of the inhibitor, was done through Eq. (4) [24]:

$$I_{corr} = K_{exp}\left(\frac{-E_a}{RT}\right) \quad (4)$$

where i_{corr} is the current density (A.cm^{-2}), K is pre-exponential constant, E_a is the activation energy (kJ. mol^{-1}), R is the UGC (8.31 J mol^{-1}. K^{-1}), and T is the absolute temperature in K.

Figure 6 displays the deviation of Log (i_{corr}) as a function of the inverse of the temperature (1/T) for Sn in

© 2020 The Authors. Published by Wiley-VCH GmbH

0.2 M maleic acid without and with the presence of 0.02 M of HPO_4^{2-} inhibitor ions. Examining Figure 6 shows that the relation of Log (i_{corr}) = f (1000/T) is linear and follows the Arrhenius law both in the absence and presence of HPO_4^{2-} ions.

The exploitation of these curves permits us to determine the values of E_a from the slope and the pre-exponential factor from the ordinate at the origin. The activation energy value attained in the presence of the inhibitor is $E_{a(inh)} = 26.69\ kJ.mol^{-1}$, but, in the absence of the inhibitor, the value changed to $E_a = 3.21\ kJ\,mol^{-1}$.

A comparison of the activation energies obtained in the presence ($E_{a(inh)}$) and the absence (E_a) of the inhibitor indicates that $E_{a(inh)} > E_a$, which is a proof that the HPO_4^{2-} ions protect the Sn by adsorbing on the surface via electrostatic interactions. Nevertheless, this kind of temperature-sensitive bonding does not offer effective protection against corrosion at higher temperatures, as reported in the literature [25]. The increase of activation energy due to the use of inhibitor leads to a decrease in the corrosion rate of the tin metal.

3.2.3 Adsorption Isotherms

Adsorption isotherms are plots that characterize the deviation in the amount of adsorbate (inhibitor) adsorbed on the metal surface (adsorbent), which can be reflected as replacing the water molecules at the rusting sites by the molecules of the applied inhibitor [26].

The EIS data was utilized to estimate the surface coverage of the tin electrode (θ) at different HPO_4^{2-} inhibitor concentrations. The data were verified graphically by fitting to various isotherms including Langmuir and Temkin representations, as shown in Figures 7.a, and 7.b, respectively. According to these isotherms, θ is correlated to the inhibitor concentration C_{inh} via the following equations:

$$\frac{C_{inh}}{\theta} = C_{inh} + \frac{1}{K_{ads}} \quad \text{(Langmuir isotherm)} \tag{5}$$

$$\exp(-2a\theta) = K_{ads} \times C_{inh} \quad \text{(Temkin isotherm)} \tag{6}$$

where *"K"* is the binding constant of the adsorption reaction and *"a"* is the lateral interaction labeling the molecular interactions in the adsorption layer and the surface heterogeneity. The best fit was established by modeling the Langmuir isotherm (the strong correlation $R^2 = 0.9$ for both methods). The plots of C_{inh}/θ vs. C_{inh} yield a straight line, which is an indication that the adsorbing HPO_4^{2-} ions occupy typical adsorption sites at the metal/solution interface. As can be seen, by the great fit, HPO_4^{2-} ions are found to follow Langmuir adsorption isotherm (Figure 7.a).

The inhibition behavior of HPO_4^{2-} is owing to the formation of the thin film on the metal surface, as was reported by several researchers [27]. Furthermore, the metal surface in contact with the aggressive 0.2 M maleic acid solution becomes electron-deficient, where HPO_4^{2-} ions get adsorbed on the Sn metal surface to formulate a protecting complex layer.

3.3 Surface Characterization: SEM and EDX Results

SEM was used to assess the surface morphology of the Sn electrode before and after immersion in 0.2 M maleic acid solution with the absence and presence of 0.02 M HPO_4^{2-}, for 24 h, as shown by the images in Figures 8.a, and b, respectively. Figure 8.a showed the surface severe damage as visible pits on the Sn surface in the absence of HPO_4^{2-} inhibitor. However, Figure 8.b displays the intact surface with fewer pits observed in the presence of the HPO_4^{2-}inhibitor. It confirms that the metal surface is coated with the HPO_4^{2-} ions and a protective inhibitor layer was formed.

The EDX results confirmed the existence of the HPO_4^{2-} layer on the Sn surface, as seen in Figure 9. Furthermore, in the presence of HPO_4^{2-} ions, peak intensities relative to oxygen (O) significantly increased in comparison to that recorded in the absence of the inhibitor (blank solution). Furthermore, the peak relative to Phosphorus (P) appears only in the presence of HPO_4^{2-} anions in the solution. This result does not let any ambiguity on the positive effect of the HPO_4^{2-} ions on the nature of the passive layer formed on the Sn surface.

3.4 Inhibition Mechanism of Sn Corrosion by HPO_4^{2-} Ions

At higher HPO_4^{2-} ions concentration, tin corrosion is hypothetically repressed through adsorption on the bare cathodic sites and the phosphate layer, if it existed. Additionally, the inhibitor adsorption on the tin surface perhaps will hinder the metal dissolution rate by either indirectly decreasing the cathodic (and anodic) active sites (also known as the geometric blocking effect) or by varying the electrochemical reactions that occur at the tin surface/solution interface throughout the corrosion inhibition process [28].

Notably, the inhibition action and behavior of HPO_4^{2-} against Sn corrosion in 0.2 M maleic acid is similar in mechanism to the hydrogen phosphate ions inhibition mechanisms against mild steel corrosion in sodium chloride solution [27]. Figure 10 displays a schematic presentation of the proposed mechanism action of HPO_4^{2-} on the tin surface. The formation of a protection layer by on the tin metal surface the inhibitor is key to the corrosion inhibition effectiveness.

4 Conclusions

The effects of inhibitor concentration and solution temperature on inhibition efficiency of HPO_4^{2-} ions against Sn corrosion in 0.2 M maleic acid were inves-

© 2020 The Authors. Published by Wiley-VCH GmbH

tigated using different electrochemical, surface analytical, and thermodynamic techniques. The electrochemical investigations showed that the inhibition efficiency of HPO_4^{2-} ions rises sharply with increasing the inhibitor concentration and decreases with increasing the solution temperature.

Potentiodynamic polarization experiments showed that HPO_4^{2-} is a cathodic type inhibitor where the OCP was shifted to more negative values. The EIS measurement results indicated that R_{ct} values increased with higher inhibitor concentration, thus better inhibition, reaching a maximum at $C_{inh} = 2.10^{-2}$ M.

Linear fit results ($\mathbf{R}^2 = 0.9885$ and 0.9302, from the EIS and PDP, respectively) were achieved for the Langmuir adsorption isotherm, therefore typical chemisorption. This confirms that the adsorption of HPO_4^{2-} is made by the physisorption type of adsorption. Surface analytical results (SEM and EDX) showed the corrosion inhibition action of HPO_4^{2-} ions by the formation of a protective complex layer.

Acknowledgement

The authors thank the Ibn Zohr University for making all the necessary resources available for this scientific work.

References

[1] S. B. Lyon, *Corrosion of tin and its alloys*, In Shreir's Corrosion, 4th ed.; Elsevier B. V.: Amsterdam, The Netherland, **2010**, Vol. 3, pp. 2068–2077. doi:10.1016/B978-044452787-5.00099-8.
[2] D. Xia, S. Song, W. Gong, Y. Jiang, Z. Gao, J. Wang, *J. Food Eng.* **2012**, *113*, 11–18. doi:10.1016/j.jfoodeng.2012.05.035.
[3] T. Benabbouha, M. Siniti, H. El Attari, K. Chefra, F. Chibi, R. Nmila, H. Rchid, *J Bio Tribo Corros.* **2018**, *4*, 39. doi: DOIhttps://doi.org/10.1007/s40735-018-0161-0.
[4] R. B. Channouf, N. Souissi, S. Zanna, H. Ardelean, N. Bellakhal, P. Marcus, *Chemistry Africa* **2018**, *1*, 167–174. https://doi.org/10.1007/s42250-018-0011-y.
[5] S. S. Abd El Rehim, N. F. Mohamed, H. H. Hassan, *Corros. Sci.* **2004**, *46*, 1071–1082. DOI:10.1016/S0010-938X(03)00134-3.
[6] V. S. Sastri , *Corrosion Inhibitors, Principles and Applications*, Wiley, London, UK, **1998**.
[7] I. L. Rozenfeld, *Corrosion Inhibitors*, McGraw-Hill, New York, **1981**.
[8] Codex Alimentarius Commission, Organization of the UN/World Health Organization, Rome, **2001**.
[9] R. M. El-Sherif, W. A. Badawy, *Int. J. Electrochem. Sci.* **2011**, *6*, 6469–6482.
[10] F. A. Ansari, Y. S. Siddiqui, M. A. Quraishi, *Int. J. Corros. Scale Inhib.* **2019**, *4*, 816–834. doi: 10.17675/2305-6894-2019-8-4–3.
[11] S. M. Abd El Haleem, S. Abd El Wanees, E. E. Abd El Aal, A. Diab, *Corros. Sci.* **2010**, *52*, 292. https://doi.org/10.1016/j.corsci.2009.09.004.
[12] H.-W. Song, V. Saraswathy, S. Muralidharan, C. H. Lee, K. Thangavel, *Corros. Eng. Sci. Technol.* **2009**, *44*, 408–815.
[13] L. Yohai, M. Vázquez, M. B. Valcarce, *Electrochim. Acta.* **2013**, *102*, 88.
[14] L. Yohai, M. B. Valcarce, M. Vázquez, *Electrochim. Acta.* **2016**, *202*, 316.
[15] V. T. Ngala, C. L. Page, M. M. Page, *Corros. Sci.* **2003**, *45*, 1523–37.
[16] F. Simescu, H. Idrissi, *Corros. Sci.* **2009**, 51:833–40.
[17] D. Özkir, E. Bayol, A. A. Gürten, Y. Sürme, *J. Chil. Chem. Soc.* **2013**, *58*, 2158–2167. https://doi.org/10.4067/S0717-97072013000400056.
[18] A. V. Girão, G. Caputo, M. C. Ferro, *Comprehensive Analytical Chemistry, In: Characterization and Analysis of Microplastics*, (Eds): T. Rocha-Santos, A. Duarte, Elsevier, **2017**, *75*, Pp 154. DOI:10.1016/bs.coac.2016.10.002.
[19] A. da Silva, E. D'Elia, J. da Cunha Ponciano Gomes, *Corros. Sci.* **2010**, *52*, 788.
[20] S. C. Nwanonenyi, O. Ogbobe, E. E. Oguzie, *International Journal of Engineering and Technologies* **2017** *10*, 11–21.
[21] K. F. Khaled, *Corros. Sci.* **2010**, *52*, 3225.
[22] I. Obot, A. Madhankumar, *Mater. Chem. Phys.* **2016**, *177*, 266–275.
[23] P. B. Raja, A. A. Rahim, H. Osman, K. Awang, *Int. J. Miner. Metall. Mater.* **2011**, *18*, 413.
[24] J. Aljourani, K. Raeissi, M. A. Golozar, *Corros. Sci.* **2009**, *51*, 1836–1843.
[25] V. Lázárescu, O. Radovici, M. Vass, *Appl. Surf. Sci.* **1992**, *55*, 297–301. doi: 10.1016/0169-4332(92)90182-W.
[26] K. L. F. Khaled, *Int. J. Electrochem. Sci.* **2008**, *3*, 462–475.
[27] R. Mihra, A. Soni, *Indian Journal of Engineering and Materials Sciences* **2002**, *9*, 144–146.
[28] A. I. Onuchukwu, A. I. Baba, *Mater. Chem. Phys.* **1987**, *18*, 381–390.

Received: August 8, 2020
Accepted: September 2, 2020
Published online on ■■, ■■

 © 2020 The Authors. Published by Wiley-VCH GmbH

FULL PAPER

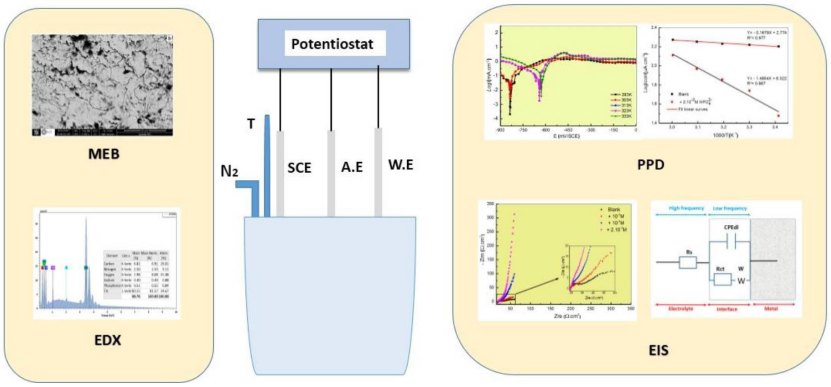

B. Ait Addi, A. Ait Addi, A. Shaban, E.-H. Ait Addi, M. Hamdani*

1 – 13

Adsorption, Thermodynamic, and Experimental Studies of Corrosion Inhibitor of Tin in 0.2 M Maleic Acid by Hydrogen Phosphate Ions (HPO_4^{2-})